Approaching Roll-to-Roll Fluidic Self-Assembly: Relevant Parameters, Machine Design, and Applications

Se-Chul Park, Jun Fang, Shantonu Biswas, Mahsa Mozafari, Thomas Stauden, and Heiko O. Jacobs, *Member, IEEE*

***Abstract*— This paper presents the implementation of an automated roll-to-roll fluidic self-assembly system based on the surface tension driven self-assembly with applications in the field of macroelectronics. The reported system incorporates automated agitation, web motion, component dispensing, and recycling. The process enables the assembly and electrical connection of semiconductor dies/chips in a continuous and parallel fashion over wide area substrates. At present, the method achieves an assembly rate of 15 000 chips per hour and an assembly yield exceeding 99%, testing assembly of standard square-shaped dies, 300–1000 μm size. Scaling the system to any desired throughput is possible due to the parallel manner of self-assembly. The identification and the modeling of the relationship between process parameters and forces have been studied and experimentally verified by testing the effect of the web angle, agitation on assembly, and detachment rates. As an application, we demonstrate the realization of a solid-state lighting module. This particular application requires the assembly of a conductive multilayer sandwich structure, which is achieved by combining the introduced assembly process with a novel lamination step. [2015-0105]**

***Index Terms*— Roll-to-roll, fluidic self-assembly, flexible electronics, solid state lighting.**

I. Introduction

THE FIELD of macroelectronics requires the integration of functional semiconductors over large area substrates in flat panel screens, large-area lighting modules, or solar panels. While the traditional microelectronics research has focused on a higher functional density and single crystal Si, the main drive for macroelectronics research has been the integration of functional materials and devices over large, flexible substrates with higher cost efficiency.

Utilized methods range from serial direct write (inkjet like) techniques and screen printing methods for organic semiconductors and hybrid organic/inorganic structure to parallel transfer [1]–[4] and self-assembly techniques [5]–[9] for inorganic materials and devices. Previous demonstrations utilizing parallel transfer [1]–[4] and self-assembly techniques [5]–[10] include flexible [11] and cylindrical displays [8], curved focal plane arrays [2], oscillators [3], RF ID tags [12], and PV modules [4] using materials such as ZnO [13], GaAs [7], [14], InP [15], GaN [16], [17], and Si [2], [3], [8], [18], [19]. In contrast to parallel transfer where functional devices are transferred from a donor wafer to a target substrate maintaining orientation and functional density, self-assembly is advantageous as it redistributes microscopic devices over large areas and order randomly distributed chips. For example, a binned container full of semiconductor dies/chiplets of a certain type and quality can be redistributed and assembled at precise locations on a substrate at any desired pitch or desired functional density using directed self-assembly. Despite of this advantage, there are only two methods available with a yield of 100%. While both methods are based on gravity, one uses shape recognition to assemble trapezoidal Si chips onto planar substrates [6], [20], [21] and the other uses surface tension driven self-assembly either using hydrophobic adhesive [22]–[24] or solder [7]–[9], [16], [25]. In our previous work, we first demonstrated an automated roll-to-roll self-assembly platform, scalable to any desired level, for assembling and electrically connecting semiconductor components in a continuous fashion [26].

In this report, we demonstrate a theoretical model for optimizing the relationship between the relevant forces and other operational parameters, and experimentally verify the evaluated results at various chip sizes. In our modeling, we utilize fluid dynamics and various effects of the web angle and agitation on assembly- and detachment rates. Our system achieves an assembly rate of ~15,000 chips per hour using a 2.5 cm wide web. This enables us to assemble square shaped chips, 300 - 1000 μm in size. Under optimized conditions, an assembly yield of 99.8% is achieved. In addition, we use a novel lamination approach in the realization of flexible solid state lighting modules incorporating distributed inorganic light emitting diodes (LEDs) using the assembly system. Since this application requires not only self-assembly, but also the formation of multilayer interconnects, the lamination approach is crucial.

Manuscript received April 23, 2015; revised June 11, 2015; accepted June 23, 2015. Date of publication July 20, 2015; date of current version November 25, 2015. This work was supported in part by the National Science Foundation under Grant DMI-1068013, in part by the Carl-Zeiss Foundation, and in part by the German Science Foundation under Grant JA 1023/3-1. Subject Editor R. T. Howe.

S.-C. Park and J. Fang are with the Department of Electrical Engineering, University of Minnesota, Minneapolis, MN 55455 USA (e-mail: parkx867@umn.edu; fang0193@umn.edu).

S. Biswas, M. Mozafari, T. Stauden, and H. O. Jacobs are with the Fachgebiet Nanotechnologie, Technische Universität Ilmenau, Ilmenau 98693, Germany (e-mail: shantonu.biswas@tu-ilmenau.de; m.mozafari@tu-ilmenau.de; thomas.stauden@tu-ilmenau.de; heiko.jacobs@tu-ilmenau.de).

Color versions of one or more of the figures in this paper are available online at http://ieeexplore.ieee.org.

Digital Object Identifier 10.1109/JMEMS.2015.2452772

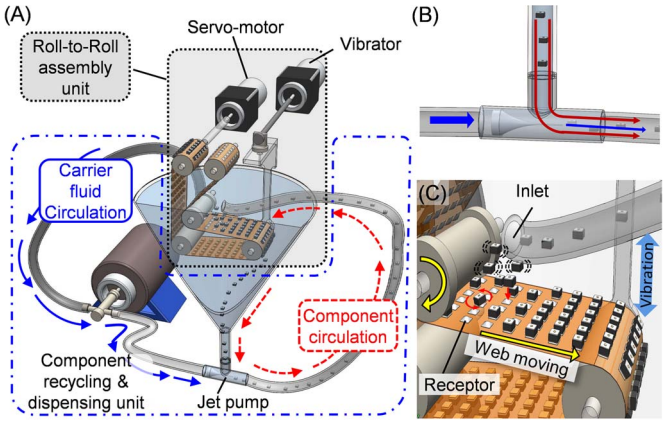

Fig. 1. Automated Roll-to-Roll fluidic self-assembly process. (A) Overview illustrating component dispensing, fluidic self-assembly based on surface tension, and recycling of excess components. (B) Principle of jet pump. (C) Illustration of surface-tension driven self-assembly using molten-solder-based-receptor.

II. Results and Discussion

A. Self-Assembly Process and Layout of Testing Platform

Fig. 1 illustrates the layout of automated roll-to-roll fluidic self-assembly system. The system contains two units:

(i) roll-to-roll assembly unit (shaded in gray) involving motor, rollers, customized agitator, and polyimide web to regulate operation parameters such as web moving speed, web angle, agitation frequency and amplitude.

(ii) component recycling and dispensing unit (shaded in blue) containing diaphragm pump, jet pump and dispensing nozzle to reintroduce and gently dispense unassembled components.

The system operation includes four steps:

(i) transporting the components to the assembly unit; a jet pump delivers the unassembled components upward into a narrow fluid channel (5 mm inner diameter tubing). Originally we installed a mechanical pump between the bottom of the chamber and the dispensing head to circulate the components, however, this lead to mechanical damage to the components and the pump. To prevent this damage, we use an indirect circulation approach coupling a mechanical pump (QV variable speed pump, Fluid metering, Inc., NY) with the customized jet pump as shown in Fig. 1(B). The jet pump requires a smaller diameter nozzle (1.48 mm^2) to accelerate the carrier fluid into a desired direction. Typical velocity of carrier fluid in the upward fluid channel (20 mm^2 tubing) is 25 cm/s to lift up the dense silicon components (density of 2.33 g/cm) to the dispensing head.

(ii) dispensing the transported components on the substrate; the components are dispensed on top of the substrate by gravity. Gentle introduction of components to the receptor is important to reduce the effect of liquid flow which induces additional drag. The dispensing head is located 5 cm away from the polyimide web (50 μm thick, 5 cm wide) pointing not directly at the web. Since the components leave the narrow dispensing head and meet large volume of liquid, the velocity decreases and the components fall downward following a vertical path to the web by gravity.

(iii) assembling the components on the substrate; the dispensed components are self-assembled on the advancing substrate. Fig. 1(C) shows the detailed attachment process. The substrates contain multiple pre-defined solder-coated receptors which are formed using a customized dip-coating of a low melting point solder on copper clad polyimide (50 μm thick, Pyralux LF series, DuPont, NC) films patterned using a microfabrication technique. Procedure to fabricate the substrate is described in the experimental section. The self-assembly process is accomplished in water at 80 °C where the solder (Indalloy #117, MP. 47 °C, Indium Corp., NY) is molten. An immersion heater is used to maintain constant temperature. The surface of the molten solder based receptor wets the gold contact of the component and the component is assembled on a stable, aligned, and electrically connected position. This assembly process is powered by minimization of the free surface area of the molten solder (400 mJ/m^2 in water). Successful self-assembly process requires removal of metal oxides from the surface of the molten solder since metal oxides impede the wetting of metal contact with the solder. This removal is accomplished by adding a few drops of hydrochloric acid to the water (pH 2.0). A web moving velocity with single dispensing head is currently 10 m/hour. As the components reach at the angled web, a uniform distribution of components is required. The described process is predominantly based on gravitational sedimentation resulting sliding and tumbling of components on the angled web. In addition, the customized vibrator can agitate the web at controlled vibration conditions through up-and-down motion of the lower roller. This additional agitation helps the distribution of the components over the web and the removal of excess components at the web turning point. The operation parameters such as the angle of web, vibration amplitude and frequency will be discussed in the results section.

(iv) collecting and recycling the unassembled components; the excess components drop down to the bottom of the chamber by gravity and are collected the T-section of the jet pump. After this point, the excess components are transported upward again and previous steps are repeated.

B. Assembly Results Using Optimized Process

Fig. 2 describes self-assembly results of various component sizes and receptor layouts including regular array and arbitrary patterns. We would test if (i) variations in size of the components would increase the number of defects and/or (ii) the position of the receptors on the substrate would affect the number of defects. Under optimal condition (will be discussed later), the defects were generally independent of the receptor position and component size. For example, Fig. 2(A)

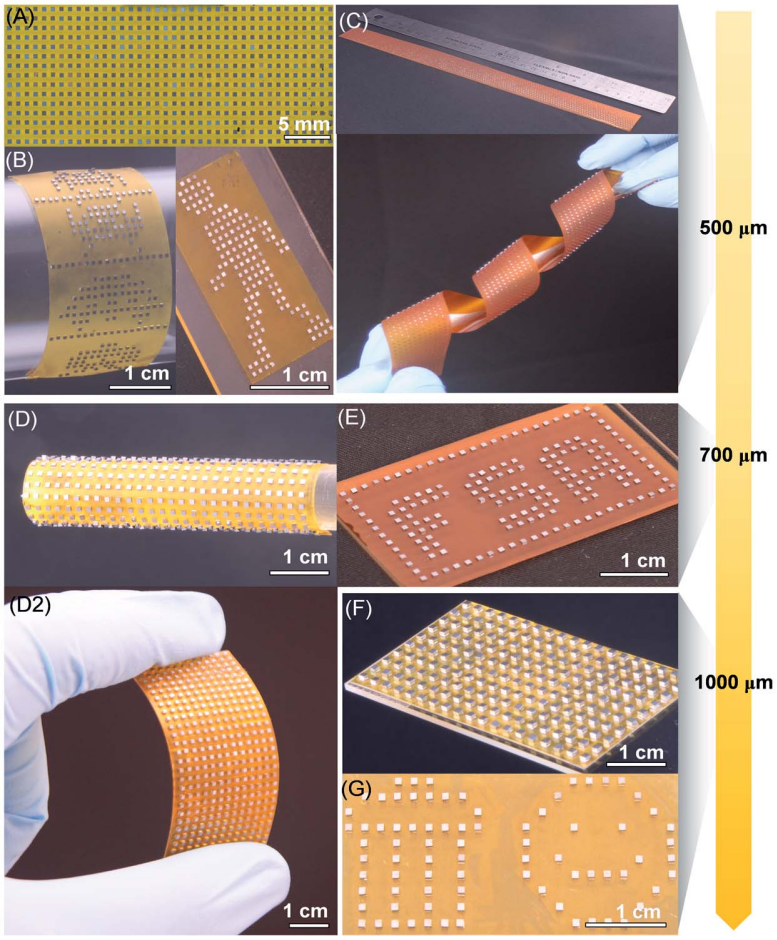

Fig. 2. Photographs showing assembly results of various sized Si components. Small (500 μm) components assemblies testing (A) periodic 1.1 mm pitched, (B) arbitrary, and (C) continuous assembly on 2 cm wide substrates (a 29 cm long section is shown). Mid-sized (700 μm) chip assemblies testing (D) periodic 1.7 mm pitched, and (E) arbitrary assemblies. Large (1000 μm) chip assemblies testing (F) periodic 2.4 mm pitched and (G) arbitrary assemblies.

depicts 570 receptors holding a single Si component where 4 misaligned components were found decreasing the yield to 99.3%; the misalignment was originated from a fabrication defect in the solder bump height, limited by manual dip-coating process not by the assembly system. Fig. 2(B) shows assembly results using arbitrary patterns which maintain the same periodicity of regular array with lower area density (42.0%, 43.9% of parts per area in (A)). There was no tendency which would indicate that the process prefers regular pattern in terms of yield. Fig. 2(C) depicts assembly results on a 29 cm $\times$ 2 cm substrate with 1523 Si components assembled in 6 min. We found 1 missing and 3 misaligned defects in this sample which reduce the yield to 99.7%. The defect positions were randomly distributed across the substrate which shows that a single nozzle can effectively spread the components over a 2 cm wide assembly area.

The use of the nozzle in combination with a tilted plane has the advantage that it can minimize shear forces when compared to prior designs [8], [27]; previously a sliding slurry of excess components inside a rotating barrel was used as a delivery mechanism; a heavy sliding slurry has the disadvantage that it can remove already assembled components leading to a deterioration of the yield. Previously such a drop in yield was observed for large (>500 μm) components as they became too heavy when compared to the restoring force of the solder connection which scales with the area of the contact pad. This is less of a challenge in the current design since we can adjust the tilt angle and the amount of excess components independently. Fig. 2(D)-(F) depict assemblies of larger chips with a side length of 700 μm and 1000 μm and chip thickness of 350 μm and 550 μm, respectively, representing a factor of 3.5 and 10 in terms of weight when compared to the Si chips with a side length of 500 μm. Fig. 2(D) depicts 351 chips with a side length of 700 μm; no missing or excess components were found. Fig. 2(F) depicts 190 chips with a side length of 1000 μm; no missing or excess components but 1 misalignment was found reducing the yield to 99.5 %. Assemblies in Fig. 2(F) and 2(G) had no defects. For reasons explained at the beginning of this paragraph it was previously [8], [27] not possible to assemble such a wide range of chip sizes. The range is presently increased by a factor of 10 in terms of weight (relevant parameter) of the chips. Further extensions of this range should be possible but we are presently limited to chips with a side

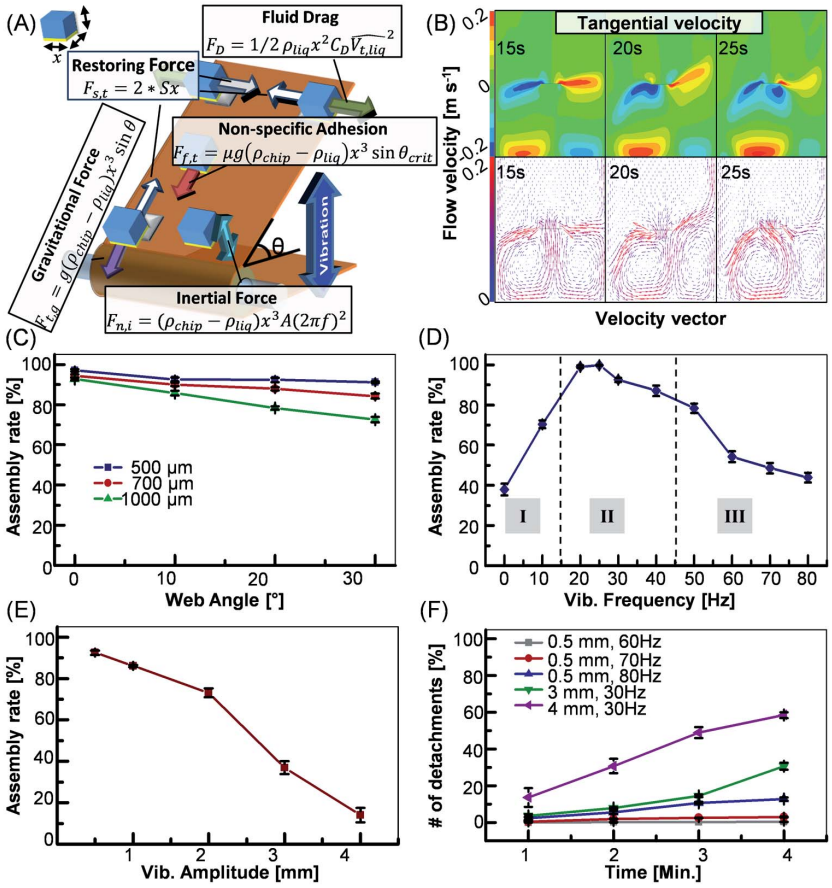

Fig. 3. Comparison of the relevant forces, fluid dynamics computation, and experimental validation. (A) Relevant forces including restoring force, gravity, non-specific adhesion, inertial and fluid drag; the inertial and fluid drag are a result of agitation. (B) Calculated fluid velocity profiles induced by a harmonic up-and-down motion of a 5 cm wide web for 15s, 20s, and 25s after the initial condition, respectively. Experimental validation and optimization testing the (C) assembly rate as a function of web angles (Average standard deviation (STD): ±0.74% for 500 μm, ±0.88% for 700 μm, ±0.99% for 1000 μm, respectively.), (D) assembly rate as a function of vibration frequency (Avg. STD: ±1.96%), (E) assembly rate as function of vibrational amplitude (Avg. STD: ±2.05%), and (F) detachment rate under excessive vibration as a function of time.

length of 300 μm - 1000 μm; smaller chips would require a higher resolution patterning methods to fabricate the solder bumps then presently used; larger chips have been tested but obstruction in the dispensing head would require a new design.

C. Relevant Forces Governing the Self-Assembly Process and Optimization

The results described in previous figure (Fig. 2) were obtained by careful optimization of the entire system looking at relevant aspects including component delivery to the web, component distribution, component assembly, and removal of excess components. The most relevant part of the optimization scheme is summarized in Fig. 3. The first part (A - B) discusses the relevant forces. The second part provides an experimental validation (C - F) and looks at the number of assembled chips in a constant time interval (referred to as assembly rate) as a function of various assembly conditions as well as the detachment rate under conditions that are not favorable to providing an insight into the details of the process.

Fig. 3(A) presents the relevant force elements, specifically:

(i) The Surface-tension-based-restoring-force ($F_{s,t}$) of a molten solder interconnect which can be calculated using $F_{s,t} = 2 * Sx$; the equation is valid if the misalignment of assembled component in the tangential direction is large compared to the solder thickness [28]. For example, the restoring force in tangential direction is approximately 400 μN considering a 0.5 mm Si cube and 400 mN/m surface tension (S) of the solder; the component in the figures are under assumption that a gravitational force or drag force cause misalignment of components; actual misalignments are much smaller than what is illustrated.

(ii) The tangential gravitational force ($F_{t,g} = g(\rho_{chip} - \rho_{liq}) x^3 \sin\theta$, roughly 1.7$\mu$N$*\sin\theta$ for a 0.5 mm Si cube) on the angled web (θ) is at least a factor of 230 smaller than the surface tension based restoring force which is also the reason why already assembled chips remain attached to the solder bumps in the upside down oriented web. However, unfavorable conditions can be used to test the effect of gravity. For example, it is

possible to load the web with a large number of excess components exceeding a single layer, under conditions of a high tilt angle, to cause a "sliding slurry" and shear forces to push assembled chips out of alignment up to a point where detachment is reached. While these effects can be reached they are not present in cases where less than a single layer of components is introduced and where the tilt angle is reduced to prevent unidirectional sliding of closely packed excess chips.

(iii) Non-specific adhesion ($F_{nonspecific\ adhesion}$) of the Si chips on the polyimide web is related since it influences the distribution of the chips. If no web vibration is used, high tilt angles are required to cause component sliding. Specifically, we observed that previously static Si cubes only begin to slide along the polyimide web at an approximate tilt angle of 48° increasing to a full sliding motion of all chips at a tilt angle of 60°. The required critical angle, where the gravity based force on the component is sufficiently strong to cause sliding of previously static chips, is important since it can be used to calculate the non-specific adhesive forces ($F_{nonspecific\ adhesion} = g(\rho_{chip}-\rho_{liq})x^3 \sin\theta_{crit}$) yielding 1.5 μN. Once in motion chips continue to slide. Under vibration, discussed later, unidirectional sliding can be observed at tilt angles down to 10°. In other words vibration can be used to achieve a slow and uniform sliding motion of the chips on the polyimide surface. For example, at a tilt angle of 10° the tangential force due to gravity is only 0.3 μN. Yet this force is sufficient to observe slow uniform downward sliding motion of 3 to 5 mm/s on an otherwise stationary web. At this speed and considering a 1 mm pitched receptor array it takes about 300 ms for an unassembled chip to reach a nearest neighbor. The sliding motion is also important considering the "residence time" which is defined as the time for a chip to be in partial contact with a 500 μm wide solder bump. The residence time is about 170 ms considering a sliding motion of 3 mm/s. A sufficiently long "residence time" is required for solder wetting to take place. Solder wetting leads to the final attachment of the chip.

(iv) The inertial force originated from the vibration of web with amplitude (A) and frequency (f) can be calculated using $F_{n,i} = (\rho_{chip}-\rho_{liq})x^3 A(2\pi f)^2$; this equation is valid when the chips contact with the web. A chip remains in contact with the web, for example, because of a solder connection (strongest, 400 μN), non-specific-adhesion (a few 1 μN), and gravitational force ($1.7\mu\text{N}*\cos\theta$). However, if the vibration frequency or amplitude exceeds critical values, separation and hopping will occur. For example, 3.0 μN (larger than gravity acting on a 0.5 mm Si cube) would be reached using 0.5 mm amplitude, 30Hz oscillation which is experimentally feasible. As mentioned previously, the web oscillation causes a significant difference in the sliding behavior. Chips slide down even at a very low tilt angle down to 10° which can now be understood since the inertial force is sufficiently strong to overcome non-specific adhesion (estimated 1.5 μN) and gravity. At the same time this mechanism is not likely to reach a value to cause chips to detach from a solder bump; 400 μN (adhesion to a solder bump) would require us to maintain 7 cm vibration amplitude at 30Hz which is experimentally not feasible using a polyimide web immersed in water even at a high web tension due to an insufficient mechanical stiffness of the arrangement.

(v) The oscillating fluid drag force is a secondary effect that may have to be considered. The origin is also the vertical vibrational motion of the web. In general terms fluid drag is an effective form of agitation since it can be tuned over a wide range of amplitudes reaching values to move previously static chips on the polyimide surface around or to even exceed the surface tension based restoring force of an already assembled chip on the solder bump which would lead to component detachment. For example, a 0.5 mm cube exposed to a relative fluid velocity (V) of 1.6 m/s will experience 400 μN drag force (calculated using $F_D = 0.5\rho_{liq}x^2C_DV^2$, with $C_D = 1.27$ and $\rho_{liq} = 971$ kg/m at 80 °C; the quadratic drag equation [29] is used rather than Stoke's drag because the calculated Reynolds number (Re) is larger than 100 regarding the experimental condition). Such a high drag force would lead to the detachment of a previously assembled chip; this is not desired but the detachment under high drag can be validated experimentally (discussed later in Fig. 3(F)). Consequently a much lower value is typically chosen to obtain high yield assemblies; at an optimized value for the liquid flow of 100 mm/s the shear force reaches 1.3 μN (calculated using $F_D = 0.5\rho_{liq}x^2C_DV^2$, with $C_D = 1$, Re = 153). A shear force value of 1.3 μN is 300 times smaller than the 400 μN restoring force of the liquid solder joint providing a sufficient safety margin to prevent component detachment. Yet such a small force is sufficient to move chips around on the surface, and it is again on the same order of magnitude than non-specific adhesion estimate (1.5 μN). Unfortunately, the liquid flow and subsequent drag force cannot be assumed constant across the surface of the oscillation web and a more precise understanding requires a somewhat complex computational fluid dynamics (CFD) analysis (Ansys CFX).

The fluid dynamics model provides a flow profile and localized flow velocities surrounding an infinitely long 5 cm wide oscillating plate excited using an optimized vibration condition used in the experiments (amplitude 0.5 mm, frequency 30Hz). The calculated fluid profile (fig. 3B) matches well with the plane stagnation flow profile [30], showing the oscillating flow in the lateral (left and right) direction near the surface of the plate. Analytical equations are used to calculate the drag force ($F_D = 0.5\rho_{liq}x^2C_DV^2$) as a result of these fluid flows, gravitational force ($F_{t,g} = g(\rho_{chip} - \rho_{liq})x^3 \sin\theta$), and non-specific adhesion force ($F_{nonspecific\ adhesion} = g(\rho_{chip}-\rho_{liq})x^3 \sin\theta_{crit}$). Typical values are listed in Table I. The first profile (left)

TABLE I
SUMMARY OF THE FORCES, THEIR RANGE, AND USE

Tangential Grav. Force $F_{t,g} = g(\rho_{chip}-\rho_{liq})x^3 \sin\theta$	**Inertial Force** $F_{n,i} = (\rho_{chi}-\rho_{liq})x^3 A\,(2\pi f)^2$	**Fluid Drag Force** $F_d = 0.5\rho_{liq}x^2 C_D V^2$	**Surface Tension** $F_{s,t} = 2 * Sx$
• **0.3 μN** at θ = 10° web angle • Chips movement: 3 mm/s with agitation • Solder contact residence time: 170 ms	• **3.0 μN** at 0.5 mm, 30Hz web vibration • Exceeding gravitational force and non-specific adhesion • Gentle lift/hopping motion of chips	• **1.3 μN** at V = 100 mm/s • 0.5 mm, 30Hz web vibration • Exceeding gravitational force and non-specific adhesion	
• **1.5 μN** at θ = 60° web angle • Chips movement: 40 mm/s with agitation. • Solder contact residence time: 12.5 ms (too short to capture chips)	• **24 μN** at 4 mm, 30Hz web vibration • Significant lift/hopping motion • Capture rate and speed of self-assembly is reduced	• **80 μN** at V = 750 mm/s • 4 mm, 30Hz web vibration • detachment of previously assembled chips was observed	**400 μN** used to capture x = 500 μm sized chips
• **1.7 μN** at θ = 90° web angle • Chips movement: 100 mm/s with agitation. • Chips are not captured.	• **400 μN** at 7 cm, 30Hz web vibration • Detachment would occur	• **400 μN** at V = 1.6 m/s • Detachment would occur	

* not yet tested due to an insufficient mechanical stiffness of the arrangement.

represent a liquid motion which is close to a published time independent flow profile surrounding an infinitely large extended plane [30]. However, our web has a finite width and is in oscillatory motion; consequently a direct comparison to a time independent study cannot be justified. As a consequence a variable moving finite element mesh method is used to determine if there are changes in the liquid velocity profile over time. Boundary layers and dimensions are identical to the experimental conditions with the exception that the web and container was assumed to be infinitely long to reduce the problem to a 2D computation. The provided URL[1] links to a video which shows the progression of the liquid flow over a period of 26 s. Three frames are shown in the Fig. 3B. First, the normal component of the liquid velocity on the surface of the web reaches the 100 mm/s peak value matching the speed of the oscillating web ($A*2\pi f$) which it should. Second, a tangential 30Hz oscillation of the liquid layer is observed as expected since this matches the drive frequency. Third, the tangential velocity amplitude is not constant and enhanced towards the edge of the web being at a minimum in the center which can also be expected considering the symmetry.

Finally, and this is interesting, the observed flow profile is not constant over time periods exceeding a few seconds. Instead the formation of short lived vortices can be observed which go hand in hand with shifts of the flow profile leading to higher amplitude oscillations towards the center of the web. This is importance since it explains why the chips experience a left and right vibration even in the center of the web and not only towards the edge as originally thought.

[1]http://www.ece.umn.edu/~hjacobs/videos.html

A frame-by-frame analysis provides additional insights into typical values of the amplitude (and velocity) of the tangential liquid flow ($V_{t,liq}$) in our experiments. Towards the sides of the web (within 50% of the total area) the values are typically larger (up to a factor of 2) than the amplitude (and velocity) of the web driving the motion. For example, the optimized 0.5 mm vertical 30Hz web oscillation (100 mm/s peak normal velocity) leads at times to a tangential liquid velocity amplitude of 200 mm/s. At 200 mm/s liquid velocity, a drag force of 4.7 μN would be present on a stationary chip (calculated using $F_D = 0.5\rho_{liq}x^2 C_D \widehat{V_{t,liq}}^2$, with $C_D = 1$, $Re = 306$). In the center, half of the web, 100 mm/s is observed at times. At 100 mm/s liquid velocity, a drag force of 1.3 μN would be present. In both cases the forces are larger than the non-specific adhesion which explain why chips are never stationary in the experiments and do not simply slide down in a linear trajectory but vibrate left-and-right. At the same time the forces (<5 μN) provides a sufficient safety margin to prevent detachment of already assembled chips which would require 400 μN.

Moreover, a 30Hz oscillation with a peak tangential liquid velocity amplitude of $\widehat{V_{t,liq}} = 100$ mm/s translates into a 1.2 mm back and forth tangential displacement of a liquid layer which in turn defines an envelope for chip movement to take place. In other words, the chips will follow this oscillating liquid movement with an amplitude smaller than the 1.2 mm envelope. Specifically, the chip motion needs to satisfy a nonlinear differential equation $0.5\rho_{liq}x^2 C_D\left(\widehat{V_{t,liq}}\sin(2\pi f t) - v_{chip}\right)^2 = \rho_{chip}x^3\frac{dv_{chip}}{dt}$ which describes the force balance between drag force and inertial force. A simple closed analytical solution for the

displacement of the chips (ΔX_{chip}) can only be given if we assume a step response whereby the liquid flows at a constant speed $\widehat{V_{t,liq}}/\sqrt{2}$ for a period of time $1/(2f)$ before it changes direction. Under this assumption the vibrational amplitude reduces to $\Delta X_{chip} = \frac{\widehat{V_{t,liq}}}{f\sqrt{8}} - k * \ln\left(1 + \frac{\widehat{V_{t,liq}}}{kf\sqrt{8}}\right)$, with $k = \frac{2x\rho_{chip}}{C_D\rho_{liq}}$ and ΔX_{chip} becomes 230 μm using $\widehat{V_{t,liq}} = 100$ mm/s, $f = 30$Hz, $x = 500$ μm chip size.

To summarize the previous two paragraphs, the input for the calculation was the vibration frequency and amplitude. A 0.5 mm, 30Hz vertical web oscillation will cause localized tangential liquid velocity of approximately 100 mm/s, which in turn leads to a subsequent drag force of 1.3 μN and periodic chip displacement of approximately 230 μm in case of a 500 μm sized chip; these values represent physical parameters that work well experimentally (discussed later). Higher vibrational amplitudes lead to higher velocities, tangential forces, and localized displacements; for example a 4 mm, 30 Hz oscillation increases the values to 750 mm/s, 80 μN, and 5.3 mm, respectively, which represents a condition far away from the optimum both in terms of capture rate and component detachment rate (validated in Fig. 3(D)-(E), discussed later).

Table I provides a summary of the relevant forces, their range, and use. The understanding of the various scaling laws was essential in the design and optimization of the self-assembly platform. The values with a green background represent optimized conditions for chips with a side length of 500 μm to provide assembly yields exceeding 99%.

In order to study and validate the calculated dependencies several experiments have been performed:

First, we evaluated the effect of gravity on the assembly rate (Fig. 3(C)) testing various inclined angles and three chip sizes with different weights (0.117 mg, 0.4 mg, 1.1 mg). In each experiment (5 experiments per data point) we tracked the number of assembled components for a fixed time of 3 minutes using a constant vibration (0.5 mm amplitude and 30Hz frequency). A described value of 98% indicates that 98% of the receptors carried a single component within 3 minutes while 2% of the receptors were unfilled. The effect of gravity is not very strong but cannot be neglected at the scale discussed here. In analogy to the previous section points (ii) and (iii), the reason why the capture rate shows a slight reduction using the heavier chips is due to a faster sliding motion and shorter residence time on the solder bumps particular towards higher tilt angles. As an example at a tilt of 30° the sliding speeds (determined by recording and analyzing the relative motion of the chips using a video camera) were 3 mm/s, 8 mm/s, and 14 mm/s for the 500, 700, 1000 μm sized chips, respectively. Chip detachment of previously assembled chips was not observed which agrees with the theory (previous section point (ii)) that gravitational shear forces are not strong enough to cause detachment.

Second, we examined the influence of vibration frequency (0 - 80Hz) (Fig. 3D) in consecutive experiments (5 experiments per data point) maintaining a fixed vibration amplitude (0.5 mm) and web angle (10°). Three operational windows can be defined that exhibit different assembly rates which can be explained as follows: (1) Slow vibration (0 - 10Hz, 0.5 mm, 10°) — in this region the advancement of self-assembly was slow and unsteady. In analogy to the previous section point (iii) some components did not show active movement due to the insufficient agitation; in this region, non-specific adhesion and gravity are dominant than inertial and drag force. Moreover, the poor distribution of component caused the assembly only on the center of the web. (2) Optimal assembly window (20 - 40Hz, 0.5 mm, 10°) — under this condition, the advancement of the self-assembly is optimized, components spread uniformly across the web and are not too fast for the self-assembly to take place; across the entire web a slow unidirectional sliding motion of the components is observed at about 3 mm/s; this velocity translates into a "residence" time of 170 ms considering a 500 μm sized solder bump. At 30Hz, 200 - 300 μm lateral chip vibration is observed which is caused by the oscillating shear flow of the liquid which is in close agreement with the theory (previous section point (v), predicting a chip displacement of 230 μm). (3) High vibration (50 - 80Hz, 0.5 mm, 10°) — In this regime, chips slide over the receptors but do not get captured by the solder bump as effectively as the slower moving chips. Some detachment is likely present but will be studied separately below.

Third, we evaluated the effect of vibration amplitude (0.5 - 4 mm) (Fig. 3(E)) in consecutive experiments (5 experiments per data point) maintaining a fixed frequency (30Hz) and tilt angle (10°). The first data point represents the optimal condition of the previous set of experiments where excellent spreading was obtained. An increase in amplitudes beyond the optimal value reduces the assembly rate. This trend can again be explained by components that begin to move too rapidly for capturing to take place (in analogy to the previous section points (ii) and (iii)). A second reason is that the liquid flow is increased to a point where the drag force causes the detachment of previously correctly assembled chips (in analogy to the previous section point (v)). Both effects should be present and a final experiment is required to confirm that a detachment condition can be reached.

The *final* set of experiments is used to test and confirm that component detachment can take place if the vibration is increased to a point where the liquid drag force becomes too large. The experiments start with previously perfectly assembled arrays containing 500 μm sized chips which are exposed to harsh vibration conditions without any excess chips inside the assembly system to a point where detachment can be observed. Fig. 3(F) depicts the total number of detachment events as a function of exposure time to various, including harsh vibration/fluid drag conditions. The results under harsh conditions are useful since they provide a deeper understanding as to why a drop in yield under high frequencies (Fig. 3(D)) and high amplitude (Fig. 3(E)) was recorded in the previous set of experiments. The conclusion is that the previously recorded drop in yield under adverse assembly conditions was actually due to a combination of a reduced capturing rate and increased detachment rate which both have

a negative impact on the progression of the self-assembly process.

The understanding and optimization of all parameters lead to the defect free assemblies discussed at the beginning. We think that more research is needed to understand the ultimate level of assembly speed and throughput that can be achieved which has not yet been the focus of the research. In addition, there are questions of the reliability of the electrical interconnects which need to be addressed going forward. However, the goal was to demonstrate that functional assemblies is feasible and that the self-assembly process reach the performance of serial robotic assembly. This goal has been achieved and we believe that our process can be adapted to various applications. For example, a field where assembly of functional microelectronics with high throughput is required would be particularly interesting application. One example is presented below.

D. Production of Flexible Solid State Lighting Modules

Fig. 4 shows the assembly of GaN LEDs which can be applied to produce other solid state lighting modules in a cost efficient manner. We used 115 μm tall and 300 μm $\times$ 300 μm thin GaN LEDs (XT290, Cree). Fig. 4(A) shows the process flow to fabricate the flexible solid state lighting modules: (i) Preparation of electrically isolated bottom electrode with receptors, (ii) assembly of LEDs on the bottom electrode using the fluidic self-assembly process, and (iii) lamination of top conductive film to finish the electrical connections.

First, a plain copper clad polyimide substrate (3.7 cm $\times$ 8 cm in total size, 2.3 cm $\times$ 7 cm in assembly region) was used as a support and common electrical contact to the LEDs. A spin coated 15 μm thick layer of epoxy based photoresist (SU-8 2010, MicroChem) is applied and patterned by lithography to define an array of openings to the copper for solder wetting and assembly to take place. Use of this polymer isolation layer eliminates additional electrical isolation steps and enables direct lamination of top conductive layer after the assembly process. The process of wire-bonding is not required. The solder based receptors were formed using the same dip-coating method described before.

Second, the LEDs (Fig. 4(B), top) need to be modified to ensure that the chips assemble with the correct (bottom side) contact on the substrate. This requires the application of a sacrificial 100 nm thick and sputter coated Ti anti-solder wetting layer onto the top face of the LEDs. Solder does not wet the Ti coating which ensures that the chips assemble with the correct orientation on the substrate. The Ti coating of correctly assembled LEDs is removed using a 45 second long wet chemical etch (Fig. 4(B), bottom right).

The *third* step is to laminate the top conductive film. The goal was to find an alternative electrical connecting method eliminating series wire-bonding which requires increasingly long processing time with an increase in the number of the components. Forming a direct electrical contact without conventional microfabrication process has been demonstrated by locating a metal coated silicone rubber or transferring a metal layer onto the desired substrate [1], [2], [31], [32].

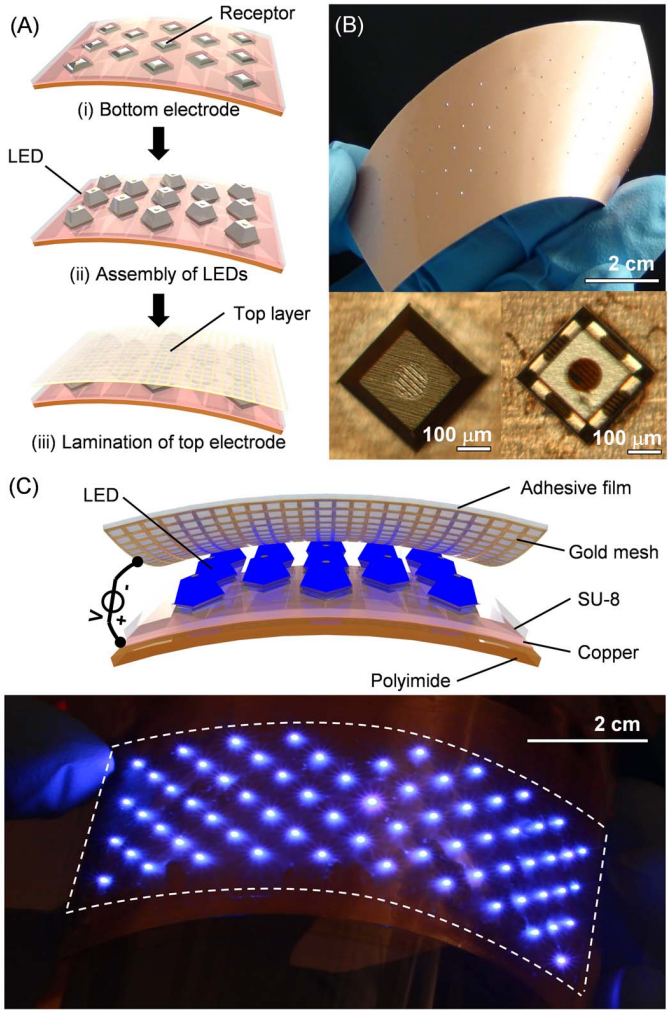

Fig. 4. Flexible solid state lighting modules realized by the roll-to-roll fluidic self-assembly platform. (A) Fabrication steps: (i) Preparation of electrically isolated flexible bottom electrode with receptors, (ii) assembly of LED using the roll-to-roll fluidic self-assembly system, and (iii) lamination of top conductive film. (B) Photograph of assembled LEDs on flexible bottom electrode, close-ups of LEDs: with an anti-solder wetting layer to control right-side-up assembly (bottom, left), and after removing the anti-solder wetting layer (bottom, right). (C) Photograph of flexible solid state lighting modules.

However, the adhesiveness of the original method based on Van-der-Waals force was not sufficient enough for certain applications. The alternative we chose has a composite structure, where parts of the surface are adhesive (and not conductive) while the rest are conductive (and less adhesive), to achieve sufficient electrical conductivity and adhesion. In the simplest form, we used a metal mesh (Fig. 4(C), top) enclosed by an adhesive surface; The Van-der-Waals adhesion between the conducting traces were sufficient to provide a small contact resistance while the surrounding adhesive stabilizes the mechanical contact between the two surfaces. To avoid critical alignment steps, we designed a mesh periodicity which is smaller than the width of the contact pad on the top of the LEDs (100 μm in our design). For example, a 25 μm pitch ensures that at least 3 horizontal and 3 vertical lines cross the top contact of the LED providing a 3 $\times$ 3 redundancy. This approach has the advantage that critical alignment is eliminated. The wire mesh can be laminated on top and will cross each contact point several times.

To test this new contact method, we fabricated a 4 cm × 7 cm gold mesh using microfabrication and transfer to a clear adhesive tape (3M Scotch tape, 3M). The composite of fabricated conducting and adhesive portions is then attached to connect the top of the LEDs. Fig. 4(C) (bottom) illustrates operation of a lighting module that consists of 67 LEDs contacted using this method. Most LEDs lit up (∼ 99%). One defect was found where no contact was made.

III. Conclusion

Herein we report the optimization of a roll-to-roll fluidic self-assembly system to assemble functional semiconductor components. Under optimized operation the system is able to assemble and electrically connect 300 - 1000 μm square components with yields approaching 100%. The optimization required a theoretical analysis and experimental validation of the relevant parameters (forces that act on the components, component transport and dispersion, and fluid dynamics calculations). The gained knowledge leads to the defect free assemblies. The system can be improved further using shape recognition to achieve contact pad registration and unique orientation [5], [9], [25] or using sequential batch assembly to integrate more than one type of components [7], [33]. Moreover, it is possible to transfer assembled chips onto other flexible or stretchable substrates. It should also be possible to extend this scheme towards smaller chip sizes in the future. Applications include flexible solid-state lighting module, large area flexible solar cell panel, and flexible energy harvesting module through integration and distribution of microscopic devices.

IV. Experimental

Si Components: To fabricate 500 μm in lateral size Si chips, 200 μm thick Si wafers (University Wafers, Boston, MA) that were cleaned with a Piranha solution (1 H_2SO_4 : 1 H_2O_2) at 120 °C for 15 min and rinsed with DI water. An e-beam evaporator was used to coat the wafer with 10 nm Cr and 200 nm Au layers. Photoresist (Microposit 1813, Shipley) was then spun on at 3,000 rpm for 30 sec. After a soft-baking, the substrate was exposed with 90 mJ/cm^2 UV light and developed in 1 Microposit 351 : 5 H_2O solution for 25 sec. The Au and Cr layers were subsequently defined using wet-chemical etching. The photoresist was stripped using acetone and a reactive ion etch (O_2, 100 sccm, 100 W, 100 mTorr). Finally, the wafer was diced using a wafer dicing saw. 700 μm and 1000 μm wide Si chips were prepared with the same conditions except the thickness of the wafers was 350 μm and 550 μm, respectively.

Self-Assembly Substrate: A copper clad polyimide is the starting material (Pyralux LF series, DuPont, NC). The 20 μm thick Cu layer was cleaned with a 1 HCl : 10 DI water solution, DI water. Dry-film (Alpha 300, Megauk, UK) was applied on the top using a tension controlled laminator at 95 °C with 250 kPa, exposed with 55 mJ/cm^2 UV light through a transparency mask, and developed in 2% K_2CO_3 in room temperature for 50 sec. The exposed Cu was wet-chemically etched in a 30% $FeCl_3$ solution for 5 min. The dry-film was removed in a 4% KOH solution at 40 °C leaving Cu squares (receptors) on the substrates. The substrate was rinsed with DI water. Finally, a low melting point solder (Indalloy #117, MP. 47 °C, Indium Corp., NY) was applied on the Cu pads through dip coating in a preheated solder bath to fabricate the predefined receptors.

SSL Application – Bottom Electrode: The fabrication of the bottom electrode uses same copper clad polyimide and follows the cleaning procedure above. Following the cleaning step, epoxy based negative photoresist is used to prevent undesired wetting of solder and electrically isolate bottom electrode from top conductive layer. SU-8 2010 (MicroChem) was spin coated onto the substrate at 2,000 rpm for 30 sec. After pre-baking at 95 °C for 3 min, the substrate was exposed with 150 mJ/cm^2 UV light and post-exposure baked at 95 °C for 3 min. The substrate was then developed in propylene glycol methyl ether acetate (PGMEA). Finally, the receptor was formed by dip-coating the solder onto the exposed copper island.

SSL Application – Top Electrode Lamination Layer: Si wafers (University Wafers, Boston, MA) that were cleaned with a Piranha solution and rinsed with DI water. 250 nm Au was the applied using an e-beam evaporator without adhesion layer. Photoresist (Microposit 1813 Shipley) was applied (3,000 rpm), exposed, and developed in Microposit 351 : 5 H_2O solution (25 sec). The Au layer was wet-chemically etched, washed in isopropyl alcohol, and carefully dried. The patterned Au mesh was transferred onto a clear adhesive tape (3M scotch tape).

References

[1] Y.-L. Loo, R. L. Willett, K. W. Baldwin, and J. A. Rogers, "Additive, nanoscale patterning of metal films with a stamp and a surface chemistry mediated transfer process: Applications in plastic electronics," *Appl. Phys. Lett.*, vol. 81, no. 3, pp. 562–564, 2002.

[2] H. C. Ko *et al.*, "A hemispherical electronic eye camera based on compressible silicon optoelectronics," *Nature*, vol. 454, pp. 748–753, Aug. 2008.

[3] D.-H. Kim *et al.*, "Complementary logic gates and ring oscillators on plastic substrates by use of printed ribbons of single-crystalline silicon," *IEEE Electron Device Lett.*, vol. 29, no. 1, pp. 73–76, Jan. 2008.

[4] J. Yoon *et al.*, "Ultrathin silicon solar microcells for semitransparent, mechanically flexible and microconcentrator module designs," *Nature Mater.*, vol. 7, pp. 907–915, Oct. 2008.

[5] S. A. Stauth and B. A. Parviz, "Self-assembled single-crystal silicon circuits on plastic," *Proc. Nat. Acad. Sci. United States Amer.*, vol. 103, no. 38, pp. 13922–13927, 2006.

[6] H.-J. J. Yeh and J. S. Smith, "Fluidic self-assembly for the integration of GaAs light-emitting diodes on Si substrates," *IEEE Photon. Technol. Lett.*, vol. 6, no. 6, pp. 706–708, Jun. 1994.

[7] W. Zheng, P. Buhlmann, and H. O. Jacobs, "Sequential shape-and-solder-directed self-assembly of functional microsystems," *Proc. Nat. Acad. Sci. United States Amer.*, vol. 101, no. 35, pp. 12814–12817, 2004.

[8] H. O. Jacobs, A. R. Tao, A. Schwartz, D. H. Gracias, and G. M. Whitesides, "Fabrication of a cylindrical display by patterned assembly," *Science*, vol. 296, no. 5566, pp. 323–325, 2002.

[9] W. Zheng and H. O. Jacobs, "Self-assembly process to integrate and connect semiconductor dies on surfaces with single-angular orientation and contact-pad registration," *Adv. Mater.*, vol. 18, no. 11, pp. 1387–1392, 2006.

[10] M. Mastrangeli, S. Abbasi, C. Varel, C. Van Hoof, J.-P. Celis, and K. Böhringer, "Self-assembly from milli- to nanoscales: Methods and applications," *J. Micromech. Microeng.*, vol. 19, no. 8, p. 083001, 2009.

[11] G. P. Crawford, "A bright new page in portable displays," *IEEE Spectr.*, vol. 37, no. 10, pp. 40–46, Oct. 2000.

[12] P. Liu, S. Ferguson, D. Edwards, and Y. Sasaki, "Radio frequency identification device and method," U.S. Patent 6 867 983, Aug. 7, 2002.

[13] J. J. Cole, X. Wang, R. J. Knuesel, and H. O. Jacobs, "Patterned growth and transfer of ZnO micro and nanocrystals with size and location control," *Adv. Mater.*, vol. 20, no. 8, pp. 1474–1478, 2008.
[14] Y. Sun, S. Kim, I. Adesida, and J. A. Rogers, "Bendable GaAs metal-semiconductor field-effect transistors formed with printed GaAs wire arrays on plastic substrates," *Appl. Phys. Lett.*, vol. 87, no. 8, pp. 083501-1–083501-3, 2005.
[15] Y. Sun and J. A. Rogers, "Fabricating semiconductor nano/microwires and transfer printing ordered arrays of them onto plastic substrates," *Nano Lett.*, vol. 4, no. 10, pp. 1953–1959, 2004.
[16] W. Zheng and H. O. Jacobs, "Shape-and-solder-directed self-assembly to package semiconductor device segments," *Appl. Phys. Lett.*, vol. 85, no. 16, pp. 3635–3637, 2004.
[17] K. J. Lee *et al.*, "Bendable GaN high electron mobility transistors on plastic substrates," *J. Appl. Phys.*, vol. 100, no. 12, pp. 124507-1–124507-4, 2006.
[18] M. A. Meitl *et al.*, "Transfer printing by kinetic control of adhesion to an elastomeric stamp," *Nature Mater.*, vol. 5, no. 1, pp. 33–38, 2006.
[19] Z.-T. Zhu, E. Menard, K. Hurley, R. G. Nuzzo, and J. A. Rogers, "Spin on dopants for high-performance single-crystal silicon transistors on flexible plastic substrates," *Appl. Phys. Lett.*, vol. 86, no. 13, pp. 133507-1–133507-3, 2005.
[20] J. S. Smith and H.-J. J. Yeh, "Method and apparatus for fabricating self-assembling microstructures," U.S. Patent 5 824 186 A, Oct. 20, 1998.
[21] R. G. Stewart and J. S. Smith, "Methods and apparatuses to identify devices," U.S. Patent 6 988 667, May 30, 2002.
[22] U. Srinivasan, D. Liepmann, and R. T. Howe, "Microstructure to substrate self-assembly using capillary forces," *J. Microelectromech. Syst.*, vol. 10, no. 1, pp. 17–24, Mar. 2001.
[23] U. Srinivasan, M. A. Helmbrecht, C. Rembe, R. S. Müller, and R. T. Howe, "Fluidic self-assembly of micromirrors onto microactuators using capillary forces," *IEEE J. Sel. Topics Quantum Electron.*, vol. 8, no. 1, pp. 4–11, Jan./Feb. 2002.
[24] K. F. Böhringer, U. Srinivasan, and R. T. Howe, "Modeling of capillary forces and binding sites for fluidic self-assembly," in *Proc. 14th IEEE Int. Conf. Micro Electro Mech. Syst.*, Interlaken, Switzerland, Jan. 2001, pp. 369–374.
[25] W. Zheng and H. O. Jacobs, "Fabrication of multicomponent microsystems by directed three-dimensional self-assembly," *Adv. Funct. Mater.*, vol. 15, no. 5, pp. 732–738, 2005.
[26] S.-C. Park, J. Fang, S. Biswas, M. Mozafari, T. Stauden, and H. O. Jacobs, "A first implementation of an automated reel-to-reel fluidic self-assembly machine," *Adv. Mater.*, vol. 26, no. 34, pp. 5942–5949, 2014.
[27] J. Chung, W. Zheng, T. J. Hatch, and H. O. Jacobs, "Programmable reconfigurable self-assembly: Parallel heterogeneous integration of chip-scale components on planar and nonplanar surfaces," *J. Microelectromech. Syst.*, vol. 15, no. 3, pp. 457–464, Jun. 2006.
[28] J. Berthier, S. Mermoz, K. Brakke, L. Sanchez, C. Frétigny, and L. Di Cioccio, "Capillary self-alignment of polygonal chips: A generalization for the shift-restoring force," *Microfluid. Nanofluid.*, vol. 14, no. 5, pp. 845–858, 2013.
[29] D. Laskovski, P. Stevenson, and K. P. Galvin, "Lift and drag forces on an isolated cubic particle in pipe flow," *Chem. Eng. Res. Design*, vol. 87, no. 12, pp. 1573–1581, 2009.
[30] R. L. Panton, *Incompressible Flow*, 3rd ed. Hoboken, NJ, USA: Wiley, 2005, pp. 235–240.
[31] H. O. Jacobs and G. M. Whitesides, "Submicrometer patterning of charge in thin-film electrets," *Science*, vol. 291, no. 5509, pp. 1763–1766, Mar. 2001.
[32] H. C. Ko *et al.*, "Curvilinear electronics formed using silicon membrane circuits and elastomeric transfer elements," *Small*, vol. 5, no. 23, pp. 2703–2709, 2009.
[33] X. Xiong *et al.*, "Controlled multibatch self-assembly of microdevices," *J. Microelectromech. Syst.*, vol. 12, no. 2, pp. 117–127, Apr. 2003.

Se-Chul Park received the B.S. degree in biochemistry and the M.S. degree in mechanical engineering from Yonsei University, Seoul, Korea, in 2005 and 2008, respectively. He is currently pursuing the Ph.D. degree in electrical engineering with the University of Minnesota, Minneapolis.

His research at the University of Minnesota focuses on engineered self-assembly, chip-scale heterogeneous integration, large-area flexible electronics, and nanotechnology.

Jun Fang received the B.S. degree in electronic and information engineering from Beihang University, China, in 2008, and the M.S. degree in electrical engineering from the University of Minnesota–Twin Cities, USA, in 2012. He is currently pursuing the Ph.D. degree in electrical engineering at the University of Minnesota.

His research at the University of Minnesota focuses on micro/nanotechnology, integration of nanoparticles/nanowires, and engineered self-assembly.

Shantonu Biswas received the B.Sc. (Hons.) degree in physics from the Shahjalal University of Science and Technology, Sylhet, Bangladesh, in 2010, and the M.Sc. degree in physics from Lund University, Lund, Sweden, in 2013. He is currently pursuing the Ph.D. degree with the Faculty of Nanotechnology, Technical University of Ilmenau, Ilmenau, Germany.

His current research focus has been to develop stretchable printed circuit board technology based on conventional fabrication process.

Mahsa Mozafari received the Diploma degree in nanostructure and molecular science from the University of Kassel, Germany, in 2012. She is currently pursuing the Ph.D. degree with the Department of Nanotechnology, Technical University Ilmenau, Germany.

Her current research includes integration of semiconductor devices on large and flexible substrates by means of fluidic self-assembly.

Thomas Stauden received the Diploma (Dipl.-Ing.) degree in electrical engineering from the Technical University of Ilmenau, Germany, in 1979, and the Ph.D. (Dr.Ing.) degree in microelectronics from the Technical University of Ilmenau, in 1986. He is currently a Coworker with the Faculty of Electrical Engineering, Technical University of Ilmenau. In 2012, he joined the Nanotechnology Group of Prof. H. O. Jacobs at the Technical University of Ilmenau. He is responsible for semiconductor technologies like plasma etching, physical vapor deposition, Molecular beam epitaxy, and rapid thermal processing. He focuses on the research on chip self-assembly processes and processes for the nanodeposition.

Heiko O. Jacobs received the M.Sc. degree in electrical engineering from the University of Wuppertal, Germany, in 1995, and the Dr.sc.Techn. degree in engineering from the Swiss Federal Institute of Technology (ETH), Switzerland, in 1999. He joined the University of Minnesota in 2001, as a Faculty Member, and an Assistant Professor after completing postdoctoral research in Harvard University with Prof. G. M. Whitesides. Since 2011, he has been the Director of the Nanotechnology Group with the Technical University of Ilmenau (TU Ilmenau). During his academic career, he carried out his research in different departments–chemistry (Harvard), mechanical engineering (ETH), physics (ETH), and electrical engineering (ETH, University of Minnesota, TU Ilmenau)–carrying out interdisciplinary research in areas of micro- and nanotechnology.